

Improved walker population control for full configuration interaction quantum Monte Carlo

Mingrui Yang,^{1,2,3,*} Elke Pahl,^{4,3,5,6,†} and Joachim Brand^{1,2,6,‡}

¹New Zealand Institute for Advanced Study and Centre for Theoretical Chemistry and Physics, Massey University, Auckland 0632, New Zealand

²Dodd-Walls Centre for Photonic and Quantum Technologies, Dunedin 9056, New Zealand

³MacDiarmid Institute for Advanced Materials and Nanotechnology, Wellington 6140, New Zealand

⁴Department of Physics, University of Auckland, Auckland 1010, New Zealand

⁵School of Natural and Computational Sciences, Massey University and Centre for Theoretical Chemistry and Physics, Auckland 0632, New Zealand

⁶Max Planck Institute for Solid State Research, Heisenbergstraße 1, 70569 Stuttgart, Germany

(Dated: June 12, 2022)

Full configuration interaction quantum Monte Carlo (FCIQMC) is a stochastic approach for finding the ground state of a quantum many-body Hamiltonian. It is based on the dynamical evolution of a walker population in Hilbert space, which samples the ground state configuration vector over many iterations. Here we present a modification of the original protocol for walker population control of Booth *et al.* JCP **131**, 054106 (2009) in order to achieve equilibration at a pre-defined average walker number and to avoid walker number overshoots. The dynamics of the walker population is described by a noisy damped harmonic oscillator and controlled by two parameters responsible for damping and forcing, respectively. We demonstrate the features of the new population control procedure such as precise walker number control and fast equilibration. The standard error of the shift estimator for the ground state energy is found to be unaffected by the population control procedure or its parameters. The improved control of the walker number, and thereby memory consumption, is a desirable feature required for automating FCIQMC calculations and requires minimal modifications to existing code.

I. INTRODUCTION

Quantum Monte Carlo methods have proven invaluable tools for providing accurate results for strongly-correlated quantum many-body problems in different areas of physics and chemistry [1–4]. One of the most straightforward approaches to solve a quantum problem with a definite particle number is to build a matrix representation of the Hamiltonian in a Fock basis, i.e. the properly symmetrized or anti-symmetrized product wave functions of N bosonic or fermionic quantum particles, respectively, in a finite number M of single-particle modes. Diagonalizing this matrix to obtain the ground or excited quantum states is known as exact diagonalization or full configuration interaction [5]. The full configuration interaction quantum Monte Carlo (FCIQMC) method [6] is a particular protocol to sample the ground state eigenvector stochastically and sparsely, allowing one to obtain accurate energies and properties of many-body problems with huge Hilbert-space dimension (e.g. up to 10^{108} in Ref. [7]). In such problems neither the matrix nor the full ground state vector could be stored in computer memory at one time. FCIQMC is classified as a projector quantum Monte Carlo approach [8] aimed at approximating the ground state, although variations of the FCIQMC protocol have been introduced to compute excited states [9], finite-temperature problems [10] with density matrices [11], transcorrelated non-hermitian Hamiltonians with three-body interactions [12–14], real-time evolution [15, 16], and driven-dissipative problems for open quantum systems [17]. The method itself is fairly

young and under active development [18–25].

During an FCIQMC simulation, the quantum state is represented, at any one time, by a set of discrete walkers or *psi*-particles, which have to be represented in computer memory [6]. Storing these walkers presents the primary memory requirement for large-scale simulations. While the storage of walkers that share the same configuration can be optimized, and walker storage can be distributed over many compute nodes in a high-performance computing environment [18], the total number of walkers that can be used is limited by the memory hardware resources. On the other hand it is usually desirable or even required to work with as large walker numbers as possible. Large walker numbers may be required to mitigate the sign problem by enabling annihilation of walkers with different signs [6, 26], to eliminate a systematic bias if the initiator approximation is used [21, 22], or simply to reduce statistical noise in estimators for desired observables like the ground state energy.

In the original FCIQMC algorithm [6] the walker number is controlled by an energy shift parameter S and there are two stages of walker population dynamics during the time evolution through iterations: In the first stage the shift is kept at a constant value S_0 and the number of walkers N_w is allowed to grow exponentially up to a threshold value N_{cut} . In the second stage the shift is updated dynamically to counteract the growth of the walker number, controlled by a damping parameter ζ . In the long-time limit the walker number will settle to fluctuate around a mean value

$$\overline{N_w} \approx N_{\text{cut}} \exp \left[\frac{(S_0 - E_0) \delta \tau}{\zeta} \right], \quad (1)$$

as is shown in this work, where $\delta \tau$ is a time-step parameter. The final mean value $\overline{N_w}$ is larger than the preset value for N_{cut} and depends on the *a priori* unknown value of the ground state

* M.Yang4@massey.ac.nz

† Elke.Pahl@auckland.ac.nz

‡ J.Brand@massey.ac.nz

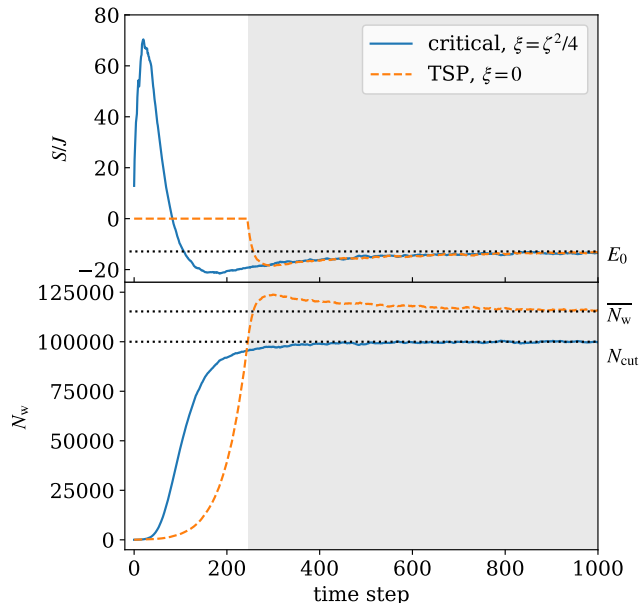


FIG. 1. Walker population control in the two-stage procedure (TSP) used in the original FCIQMC [6], where $\xi = 0$, and the single-stage procedure of Eq. (4) with the restoring force set to critical damping ($\xi = \zeta^2/4$). The top panel shows the shift and the dotted line indicates the value of the exact ground state energy E_0 . The walker number is shown in the bottom panel. Without the restoring force, the maximum of the walker number reaches $N_{w,\max} \approx 124,000$ and later equilibrates to $\bar{N}_w \approx 115,000$ indicated by the upper dotted line. The value of $N_{\text{cut}} = N_t = 10^5$ is indicated by the lower dotted line. We have chosen a time step of $\delta\tau = 0.001J^{-1}$ and set the damping parameter to $\zeta = 0.08$ for both procedures. Parameters of the Bose-Hubbard model are $U/J = 6$, $N = M = 20$.

energy E_0 . Moreover, it is possible to get overshoots, where the walker number significantly exceeds both the target value N_{cut} and the final mean value \bar{N}_w at intermediate times before settling to fluctuate around \bar{N}_w . An example of such behavior is shown in Fig. 1, where the dashed orange lines show the evolution of the shift S (top) and walker number N_w (bottom) in the two-stage procedure of Ref. [6]. The fact that the maximum and final average number of walkers are not directly determined by the parameters of the simulations complicates the planning of computational resources and may be met with an over-allocation of resources or requires elaborate estimation or multi-step procedures. A tighter control of the walker number with a pre-defined target value is clearly desirable.

In this work we propose a modified population control procedure for FCIQMC by introducing an additional “forcing” term characterized by a parameter ξ and a target walker number N_t . The new term represents a restoring force that will push the walker population towards the target value N_t . The behavior of the new procedure is shown in Fig. 1 by the full blue lines, where the shift is adjusted from the beginning of the simulation and the walker number quickly equilibrates around the pre-defined value N_t . Analysing the population dy-

namics by a simplified scalar model reveals that the logarithm of the walker number follows the dynamics of a damped harmonic oscillator equilibrating at $N_w = N_t$. The walker number control in the original FCIQMC [6] corresponds to the special case without restoring force. A more detailed discussion of Fig. 1 will follow in Sec. V.

This paper is organised as follows: After introducing the FCIQMC algorithm with modified walker population control in Sec. II we briefly introduce the model and computational details in Sec. III. In Sec. IV we derive the scalar differential equation model for the walker dynamics and discuss the solutions with and without forcing term. Walker number overshoots and long-time limits are discussed in Sec. V where we also derive Eq. (1). Section VI deals with fluctuations in the equilibrium phase of the simulation and examines the influence of the damping parameter and parameters of the model Hamiltonian before concluding in Sec. VII. Details of the Bose-Hubbard model are presented in Appendix A.

II. WALKER POPULATION CONTROL IN FCIQMC

In the configuration interaction approach, the many-body quantum state or wave function is represented by a vector \mathbf{c} composed of coefficients that give the signed weights of individual Fock states, or configurations. Correspondingly, the quantum Hamiltonian is represented by a matrix \mathbf{H} . The FCIQMC algorithm is based on the iterative equation describing the update of the coefficient vector $\mathbf{c}^{(n)}$ at the n -th time step in discrete time steps $\delta\tau$:

$$\mathbf{c}^{(n+1)} = [\mathbb{1} + \delta\tau(S^{(n)}\mathbb{1} - \mathbf{H})]\mathbf{c}^{(n)}. \quad (2)$$

Here $\mathbb{1}$ represents the unit matrix, $S^{(n)}$ is the energy shift at time step n , and we use units where $\hbar = 1$. The iteration prescription of Eq. (2), if performed exactly, will make the vector $\mathbf{c}^{(\infty)}$ proportional to the ground state eigenvector, the dominant eigenvector of $-\mathbf{H}$. The procedure can be understood either as a repeated matrix-vector multiplication and variant of the power method, or as executing Euler steps of the discretized imaginary time evolution in the Schrödinger equation. The actual FCIQMC algorithm is a stochastic procedure involving discrete walkers that is aimed to solve Eq. (2) on average [6, 18]. The coefficient vector \mathbf{c}^n at any one time is made up of integer numbers and its one-norm $\|\mathbf{c}\|_1 \equiv \sum_i |c_i|$ is interpreted as the number of walkers N_w . Representing the coefficients as integers and controlling the total number $N_w = \|\mathbf{c}\|_1$ allows for a sparse representation of the coefficient vector, where only non-zero elements have to be stored in memory. This is particularly efficient in the typical scenario where the dimension of the linear space is much larger than the number of walkers. The walker number N_w thus controls the demand for physical memory consumption of an FCIQMC simulation. While the notion of integer walkers was relaxed to include fractional walkers, and floating-point coefficients in a limited subspace of Hilbert space in the context of semi-stochastic FCIQMC [19, 20], the basic principle remains the same. The walker number (defined by the one-norm $N_w = \|\mathbf{c}\|_1$) still controls the

memory consumption in addition to demands for representing the deterministic space.

In order to control the number of walkers, the original FCIQMC algorithm [6] proposed a two-stage procedure

$$S^{(n)} = S_0 \quad \text{Stage 1,} \quad (3a)$$

$$S^{(n+A)} = S^{(n)} - \frac{\zeta}{A\delta\tau} \ln \left(\frac{N_w^{(n+A)}}{N_w^{(n)}} \right) \quad \text{Stage 2.} \quad (3b)$$

During Stage 1 the shift is kept at a constant value S_0 , usually set to the lowest diagonal matrix element of \mathbf{H} , in order to let the walker number grow from a small starting value until it reaches a threshold value N_{cut} . After the threshold is reached, Stage 2 is activated and the shift is updated every A time steps according to Eq. (3b), where ζ is a dimensionless damping parameter and parameter ranges of $\zeta = 0.05\text{--}0.1$ and $A = 5\text{--}10$ are proposed in Ref. [6]. The shift update procedure counteracts any exponential growth of the walker number caused by Eq. (2) by lowering the shift, and conversely also counteracts exponential damping by raising the shift S . An equilibrium is reached when the coefficient vector $\mathbf{c}^{(n)}$ is proportional to the ground state vector \mathbf{c}_0 and the shift equal to the ground state energy, $S = E_0$. A steady state is reached where neither the walker number nor the shift changes. In the typical case where the stochastic realisation of Eq. (2) introduces noise, both the shift and the walker number will fluctuate around their equilibrium values. The equilibrium value of the walker number is not predefined in the procedure of Eq. (3) but depends on the initial conditions.

Motivated by the walker control mechanism in diffusion Monte Carlo, where an energy control parameter is adjusted when the walker number deviates from a target value [27], we propose the following modified shift-update procedure

$$S^{(n+A)} = S^{(n)} - \frac{\zeta}{A\delta\tau} \ln \left(\frac{N_w^{(n+A)}}{N_w^{(n)}} \right) - \frac{\xi}{A\delta\tau} \ln \left(\frac{N_w^{(n+A)}}{N_t} \right), \quad (4)$$

which reduces to the original update equation (3b) for $\xi = 0$. The dimensionless parameter ξ represents a forcing strength and N_t is the target walker number. It is easily seen that under steady-state conditions the last two terms must vanish and thus the walker number will equilibrate at the target walker number N_t . In contrast to the original FCIQMC procedure where the shift is updated only after a threshold number of walkers has been reached, the new shift update procedure of Eq. (4) can be used from the start of a simulation, even if the initial walker number is very different from the desired final number N_t . In the remainder of this paper, for analysis and also for numerical examples we set $A = 1$. I.e. that the shift is updated in every time step for simplicity, although similar delayed shift updates as suggested in Ref. [6] could be performed.

III. SIMULATION DETAILS

All FCIQMC simulations for this paper were done on the Bose-Hubbard model [28], which is relevant to ultra-cold

atom experiments in optical lattices [29–32]. We use a one-dimensional configuration with periodic boundary conditions. The Hamiltonian and details of the model are summarised in Appendix A. The simulations were performed with the library `Rimu.jl` written in the programming language Julia by the authors for FCIQMC with bosonic many-body models. `Rimu.jl` is available as open source on GitHub [33]. Implementations of FCIQMC targeting quantum chemical applications as well as the (Fermi) Hubbard model and spin models are publicly available [34, 35].

IV. SCALAR MODEL OF WALKER POPULATION DYNAMICS

We will further analyse the effects of the shift-update procedure on the dynamics of the walker number with a simple scalar model. In order to motivate the model, let us assume that the coefficient-vector update of Eq. (2) is performed exactly and that the coefficient vector is already proportional to the ground state with $\mathbf{c}^{(n)} = N_w^{(n)} \mathbf{c}_0$. Here \mathbf{c}_0 is an eigenvector of the matrix-vector equation $\mathbf{H}\mathbf{c}_0 = E_0\mathbf{c}_0$ with energy eigenvalue E_0 and $N_w^{(n)}$ the walker number in the n th time step. Then Eq. (2) reduces to a scalar update equation for the walker number

$$N_w^{(n+1)} = [1 + \delta\tau(S^{(n)} - E_0)]N_w^{(n)}. \quad (5)$$

Together with the shift update equation (4), it defines the walker number dynamics in discrete time.

Aiming at approximating this dynamics by a differential equation, we introduce a time variable $t = n\delta\tau$ and a new variable x for the logarithm of the ratio between the momentary and the target walker number

$$x^{(n)} = \ln \frac{N_w^{(n)}}{N_t} \longrightarrow x(t) = \ln \frac{N_w(t)}{N_t}. \quad (6)$$

The shift update equation (4) can be written in terms of x as

$$\frac{S^{(n+1)} - S^{(n)}}{\delta\tau} = -\frac{\zeta}{\delta\tau} \frac{x^{(n+1)} - x^{(n)}}{\delta\tau} - \frac{\xi}{\delta\tau^2} x^{(n)}, \quad (7)$$

which is a finite difference approximation of the differential equation

$$\frac{dS}{dt} = -\frac{\zeta}{\delta\tau} \frac{dx}{dt} - \frac{\xi}{\delta\tau^2} x(t). \quad (8)$$

After rearranging the walker number equation (5), it is seen to represent a finite difference approximation to the logarithmic time derivative of the walker number

$$S^{(n)} - E_0 = \frac{N_w^{(n+1)} - N_w^{(n)}}{\delta\tau N_w^{(n)}} \approx \frac{d \ln N_w}{dt} = \frac{dx}{dt}, \quad (9)$$

which yields the differential equation

$$\frac{dx}{dt} = S(t) - E_0. \quad (10)$$

Equations (8) and (10) form a set of coupled first order ordinary differential equations, which determine the time evolution of $x(t)$ and $S(t)$. By eliminating $S(t)$, the equations can further be combined into a single second order differential equation for x

$$\frac{d^2x(t)}{dt^2} + \frac{\zeta}{\delta\tau} \frac{dx(t)}{dt} + \frac{\xi}{\delta\tau^2} x(t) = 0. \quad (11)$$

This is the well-known differential equation for the damped harmonic oscillator. Here, $\zeta/\delta\tau$ represents a damping coefficient and $\xi/\delta\tau^2$ the force constant of a restoring force.

A. Walker number dynamics with forcing

The general solution of the differential equation for the damped harmonic oscillator (11) can be written as

$$x(t) = ae^{-\frac{t}{T_+}} + be^{-\frac{t}{T_-}}, \quad (12)$$

with arbitrary constants a and b whose values are determined by the initial conditions. The two independent solutions $x_{\pm}(t) = \exp(-t/T_{\pm})$ will both decay to zero in the long-time limit. The solutions for the time constant are

$$T_{\pm} = \frac{\delta\tau}{2\xi} \left(\zeta \pm \sqrt{\zeta^2 - 4\xi} \right). \quad (13)$$

Depending on the value of the discriminant $\zeta^2 - 4\xi$ we can distinguish three cases corresponding to overdamped, critical and underdamped behaviour. If $\zeta^2 > 4\xi$, the time constants are both real-valued and both fundamental solutions show exponential damping. This is the overdamped case. In the underdamped case of $\zeta^2 < 4\xi$, the square root has imaginary solutions and both fundamental solutions are products of an oscillating component and an exponential damping factor.

The case of critical damping with

$$4\xi = \zeta^2, \quad (14)$$

is of particular interest since it is the point at which the damping is the fastest. The critical damping time is given by

$$T_c = \frac{\delta\tau}{\sqrt{\xi}} = \frac{2}{\zeta} \delta\tau. \quad (15)$$

Since the exponential ansatz only provides a single fundamental solution of the second order differential equation, another independent solution has to be found. It can be easily checked that a second independent solution is $t \exp(-t/T_c)$. The general solution in the critical damping case is then given by

$$x(t) = (a + bt)e^{-\frac{t}{T_c}}. \quad (16)$$

Note that the parameters ζ and ξ are dimensionless and determine the decay time scale in units of $\delta\tau$. I.e. the number of time steps until the solution decays by a certain amount is independent of the size of the time step $\delta\tau$.

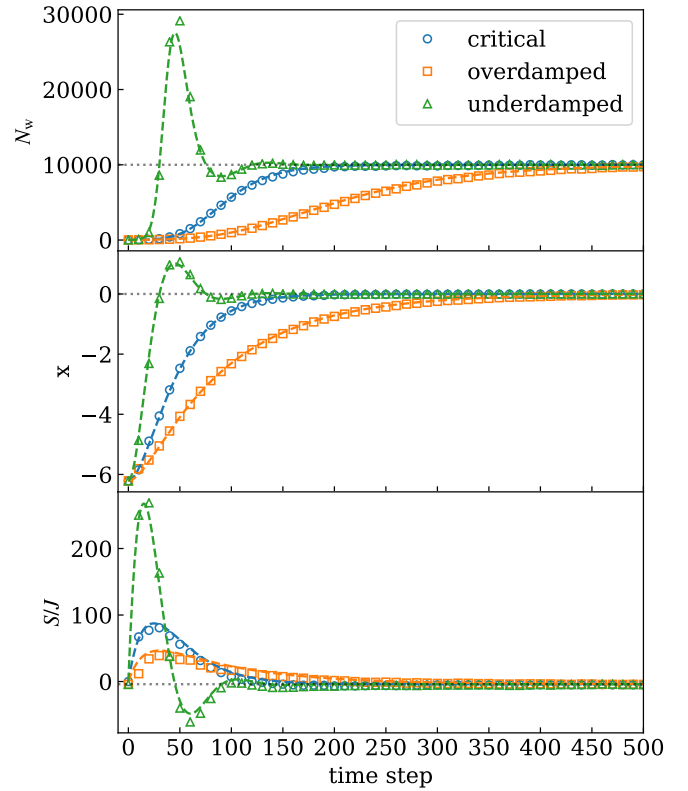


FIG. 2. Walker population dynamics in FCIQMC with the shift-update procedure of Eq. (4) (symbols) for the Bose-Hubbard model compared with the scalar model of Eq. (11) (dashed lines). The top panel shows the evolution of the walker number N_w for three different damping scenarios and the middle and bottom panels show the logarithm $x = \ln(N_w/N_t)$, and the shift S , respectively. We used $\zeta = 0.08$ and set $\xi = 0.0016, 0.0008, 0.0064$ representing the critical, overdamped, and underdamped regimes, respectively. The initial conditions were $N_w = 20$ and $S = 0$ at $t = 0$, and the target walker number was set to $N_t = 10,000$. The parameters of the Bose-Hubbard model are $M = N = 6$ and $U/J = 6$. Other parameters used are $\delta\tau = 0.001J^{-1}$, and $A = 1$. The dashed lines show the asymptotic values $N_t = 10^4$, $x = 0$, and $E_0 = -4.0J$ in panels 1, 2, and 3, respectively. The simulation data is only shown at every tenth time step for clarity.

Figure 2 shows how the analytic solutions of the scalar model (11) match FCIQMC simulations of the Bose-Hubbard model very well, demonstrating that underdamped, critical, and overdamped walker number dynamics can be achieved with the new update procedure of Eq. (4). The time evolution of the walker number is given by $N_w(t) = N_t e^{x(t)}$ according to Eq. (6). In the steady-state (long-time) limit, the solution becomes time-independent with $x = 0$, or $N_w \rightarrow N_t$. The time evolution of the shift is obtained from Eq. (10). In the long-time limit the left hand side vanishes and $S \rightarrow E_0$.

B. Walker number dynamics without forcing

In the original FCIQMC of Ref. [6], after reaching Stage 2 of the two-stage procedure (3), the evolution of shift and walker number experience damped motion without restoring force ($\xi = 0$) and thus no predefined equilibrium exists. In this case it is more convenient to write the differential equation in terms of

$$s(t) \equiv S(t) - E_0 = \frac{dx}{dt}, \quad (17)$$

which describes the deviation of the shift from the equilibrium value. Combining Eqs. (8) and (10) we then obtain

$$\frac{ds(t)}{dt} + \frac{\zeta}{\delta\tau} s(t) = 0. \quad (18)$$

This is a simple damping equation with solution

$$s(t) = [S(0) - E_0] e^{-\frac{t}{T_d}}, \quad (19)$$

with the damping time

$$T_d = \frac{\delta\tau}{\zeta}. \quad (20)$$

The time dependence for the walker number follows from Eq. ((6)):

$$N_w(t) = N_t e^{x(t)} \quad (21)$$

Choosing the time axis to start at $t = 0$ when entering Stage 2 of Eq. (3) where $N_w(0) = N_{\text{cut}}$ and $S(0) = S_0$, the exponential expression for the walker number $N_w(t)$ can be expressed as

$$N_w(t) = N_{\text{cut}} \exp \left\{ (S_0 - E_0) T_d \left[1 - \exp \left(-\frac{t}{T_d} \right) \right] \right\}. \quad (22)$$

Taking the long-time limit $t \rightarrow \infty$ and substituting Eq. (20) for T_d we obtain Eq. (1) for the final walker number.

Note that the time evolution described by Eq. (22) is monotonously growing or decaying depending on the sign of $S_0 - E_0$. In the standard procedure the initial shift is larger than the final ground state energy, in order to induce walker growth during Stage 1, and thus the scalar model predicts further growth during Stage 2 to the final larger value of Eq. (1). The damping time T_d of Eq. (20) is smaller by a factor of 2 compared to the critical damping time T_c of the damped harmonic oscillator, Eq. (15), at the same value of ζ . But this faster damping comes with the cost of reaching a final walker number that depends on the *a priori* unknown value of the ground state energy E_0 .

V. WALKER NUMBER DYNAMICS IN FCIQMC

In a real FCIQMC simulation the walker number will fluctuate due to updating the walker number with the complicated and noisy evaluation of Eq. (2). Even without forcing ($\xi = 0$)

these fluctuations do not lead to a drift in walker number but instead the walker number is seen to fluctuate around a stable average. This can be understood from the logarithmic update equation (3b), which is evaluated exactly during the simulation. The update equation (3b) can be re-written in terms of the initial conditions as

$$S^{(n+A)} = S_0 - \frac{\zeta}{A\delta\tau} \ln \left(\frac{N_w^{(n+A)}}{N_{\text{cut}}} \right), \quad (23)$$

which reveals that the value of the shift at any time during the FCIQMC simulation depends only on the initial conditions and the instantaneous walker number but not on the details of fluctuations at intermediate times. Taking the average over many time steps we obtain

$$\bar{S} = S_0 - \frac{\zeta}{\delta\tau} \overline{\ln \left(\frac{N_w}{N_{\text{cut}}} \right)}. \quad (24)$$

Replacing the average shift \bar{S} in the long-time limit with the exact ground state energy E_0 and approximating the average of the logarithm by the logarithm of the average (with an error $\mathcal{O}[\text{Var}(N_w/N_{\text{cut}})]$), we, once again, obtain Eq. (1). Note that Eq. (24) is an exact result that does not rely on the assumptions of the scalar model and fully includes the effects of a noisy simulation. This means, in particular, that the expression (1) for the final walker number is valid for FCIQMC with forceless damping even in situations where the scalar model is not sufficient to fully capture the dynamical evolution of the walker number.

In some cases we see initial growth and overshooting of the walker number before decaying to the long term limiting value as e.g. in Fig 1. Such non-monotonous behaviour of $N_w(t)$ is not captured by the scalar model solution of Eq. (22), which predicts monotonous growth. In Fig 1 the walker number for the two-stage procedure grows rapidly at the beginning of Stage 2 until saturating at a maximum on a time scale that is consistent with the damping time $T_d \approx 12.5\delta\tau$. On the same time scale the shift decays to a minimum value, where it matches the value of the shift obtained with the restoring-force (single-stage) procedure. A further equilibration of the shift to the final value E_0 then happens at a much longer time scale over hundreds of time steps for both procedures. We attribute this behaviour to the necessary equilibration of the walker distribution to better represent the ground state vector \mathbf{c}_0 . This mechanism is not captured by the simplified Eq. (5), which formed the starting point of the scalar model analysis. During this period of slow equilibration, the walker number follows the slowly changing shift adiabatically according to Eq. (24) for the two-step procedure without forcing.

The evolution of the walker number for the critical-damping update procedure seen in Fig 1 is very different though, as here the ξ term forces the walker number back to the target walker number N_t on the time scale $T_c = 25\delta\tau$. This time scale is again much faster than the time scale of rearranging the walker population, which affects the slowly changing average of the shift. The equilibration process of the walker population for FCIQMC in large Hilbert spaces was recently discussed in Ref. [36].

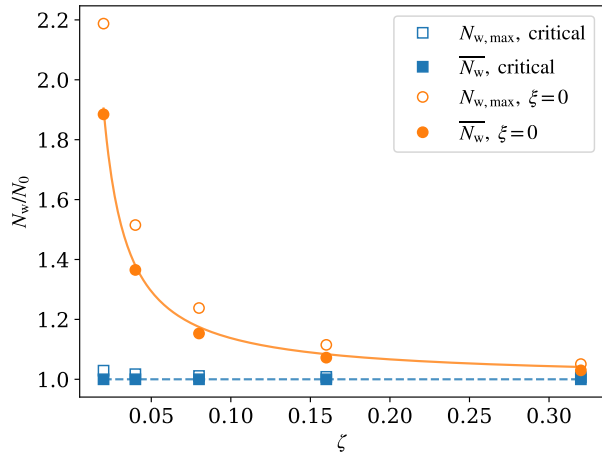


FIG. 3. Final walker number and overshoot as function of the damping parameter ζ . The maximum walker number reached during a simulation with $N_{w,\max}$ (empty markers), and the long-time average $\overline{N_w}$ (filled markers) with 10^6 time steps are shown for both the single-stage critical damping ($\xi = \zeta^2/4$) and the two-stage procedure without restoring force ($\xi = 0$) and $N_{\text{cut}} = N_0$ with $N_0 = 10^5$. The yellow solid line shows the prediction for $\overline{N_w}$ without restoring force from Eq. (1). The blue dashed line shows the prediction $\overline{N_w} \approx N_t$ for the single-step procedure with critical forcing where $\xi = \zeta^2/4$ and $N_t = N_0$. The corresponding data for the single-stage procedure is close to the prediction and reveals the superior walker number control and avoidance of overshoots compared to the unforced walker number control. The parameters of the Bose–Hubbard model are $M = N = 20$ and $U/J = 6$, and $\delta\tau = 0.001J^{-1}$. $E_0 \approx -12.88J$ was obtained from long time average of the shift.

Next, we examine the dependence of the overshoot and final walker number on the damping parameter ζ in Fig. 3. Shown are both the final average walker number $\overline{N_w}$ as well as the maximum number reached during the simulation $N_{w,\max}$, which indicates the overshoot and is the relevant number for computer memory resources. We find that the exponential dependence predicted by Eq. (1) captures the results from FCIQMC simulations of the Bose–Hubbard model very well. Equation (1) for $\overline{N_w}$ (supported by Fig. 3) then suggests that the increase in walker number beyond the threshold value N_{cut} can be mitigated by increasing the damping parameter ζ or decreasing the time step $\delta\tau$. Another possible mitigation strategy would be to set a sequence of intermediate threshold values to smaller values than the final desired value N_{cut} and alternate constant-shift and equilibration stages multiple times in order to decrease the energy difference $S_0 - E_0$ in Eq. (1). The data from FCIQMC simulations with the one-stage procedure at critical damping shown in Fig. 3 demonstrate, however, that both the final and maximum walker number can be very well controlled regardless of the other simulation parameters. Those parameters can then be chosen according to other criteria (*e.g.* larger time steps for faster convergence and better numerical efficiency).

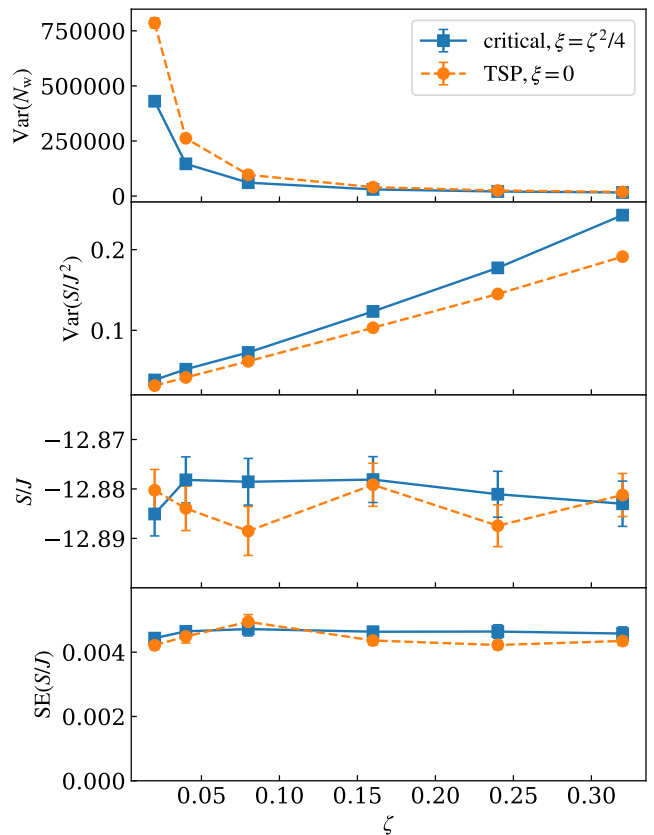


FIG. 4. Fluctuating quantities in the equilibrium phase of an FCIQMC simulation as a function of the damping parameter ζ with the restoring force set to critical damping ($\xi = \zeta^2/4$), and for the two-stage procedure (TSP) without restoring force ($\xi = 0$). The top panel shows the variance of the walker number and the second panel the variance of the shift, obtained from ten blocks of 10^5 data points each. The shift estimator in the third panel was obtained from averaging 10^6 time steps, and the standard error (shown separately in the bottom panel) was found by blocking analysis. The same average walker number $\overline{N_w} = 100,000 \pm 500$ after equilibration was used for both procedures to ensure the results are directly comparable. The parameters of the Bose–Hubbard model are set to $M = N = 20$, $U/J = 6$ and $\delta\tau = 0.001J^{-1}$. Error bars for the variances and the SE are mostly within the markers. The lines between markers are a guide to the eye.

VI. FLUCTUATIONS IN EQUILIBRIUM

After an initial phase of dynamics in the walker number and the shift, an equilibrium is reached where the walker number and the shift fluctuate around their long-time average values. The fluctuations originate in the stochastic procedure of evaluating Eq. (2). During this equilibrium phase the fluctuating coefficient vector $\mathbf{c}^{(n)}$ samples the ground state and the average of the fluctuating shift provides an estimator for the ground state energy.

A. Effect of the damping parameter

Figure 4 shows how various quantities of interest are affected by the damping parameter ζ in the equilibrium phase for both the original two-stage procedure without forcing ($\xi = 0$) and for the new procedure with the restoring force tuned to the critical value ($\xi = \zeta^2/4$). The variances in shift and in walker population, $\text{Var}(S)$ and $\text{Var}(N_w)$ respectively, are calculated as the average from ten blocks of the 100,000-step data set. A trade-off can be seen between fluctuations of the walker number, where the variance is suppressed for increasing ζ (top panel), and the fluctuations in the shift, whose variance grows with increasing ζ (second panel from top). This is not surprising, since the shift is related to the logarithmic derivative of the walker number per Eq. (10) and thus the quantities are conjugate to each other. It is also seen in Fig. 4 that the one-stage procedure with restoring force at critical value is more effective in suppressing fluctuations in the walker number than the two-stage procedure without restoring force ($\xi = 0$) at the same value of ζ , while the opposite is true for the variance of the shift. The variance of the shift is a particularly relevant quantity because the shift estimator for the ground state energy is obtained by averaging the fluctuating shift over many time steps (here 10^6). The shift estimator is shown in the third panel and it can be verified that the obtained values all agree within error bars for all values of the ζ and ξ parameters. The error bars (shown in the bottom panel) signify the standard error (SE) obtained from an automated blocking analysis, where the data is de-correlated by blocking transformations [37] and the success of the decorrelation established with the ‘‘M-test’’ method by Jonsson [38]. The approach also yields error estimates for the standard error, which are shown as error bars in the bottom panel (mostly within marker size).

The standard error of the shift estimator is an important quantity because it quantifies the quality of the Monte-Carlo simulation. It is remarkable to see that the same standard error for the shift is obtained for the different values of the damping and forcing parameters (bottom panel, Fig. 4), even though the variances of the shift vary greatly (second panel, Fig. 4). This fact can be rationalized by considering that the standard error is not only affected by the fluctuations of the shift captured by the variance but also by correlations in the time series. In particular the squared standard error of the shift estimator (i.e. the variance of the sample mean of $S^{(n)}$) is obtained from the auto-covariance $\gamma(h)$ by the sum [37]

$$[\text{SE}(S)]^2 = \frac{1}{n_d} \left[\gamma(0) + 2 \sum_{h=1}^{n_d} \left(1 - \frac{h}{n_d}\right) \gamma(h) \right], \quad (25)$$

where n_d is the number of data points. The auto-covariance of the shift is

$$\gamma(h) = \overline{(S^{(n)} - \bar{S})(S^{(n+h)} - \bar{S})}, \quad (26)$$

where $\overline{\dots}$ signifies the sample average over a sufficiently long time series of data. h is a delay in time steps and for $h = 0$ the auto-covariance becomes the variance $\gamma(0) = \text{Var}(S)$. Figure

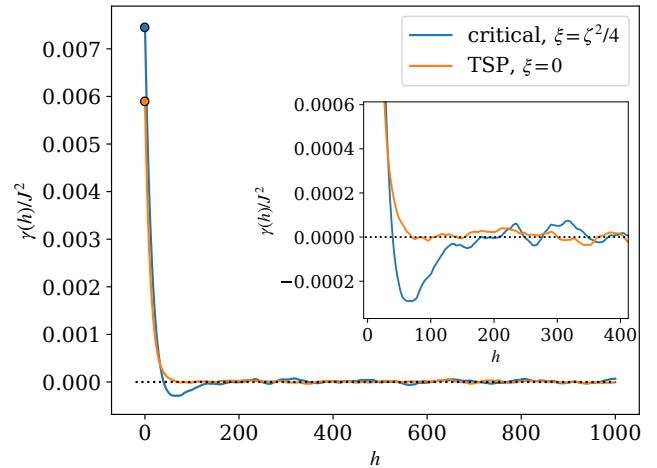


FIG. 5. Auto-covariance of the shift for the single-stage procedure with the restoring force set to critical damping ($\xi = \zeta^2/4$) and for the two-stage procedure (TSP) without restoring force ($\xi = 0$). The inset shows the details around the zero-crossing point for the critical damping curve. The parameters of the Bose–Hubbard model are set to $M = N = 6$, $U/J = 6$. The parameters used are $\delta\tau = 0.001J^{-1}$, and $\zeta = 0.08$ for both procedures. The walker population is equilibrated to $\bar{N}_w = 10^5$. Both data sets used to calculate the auto-covariance contain results from 10^6 time steps.

5 shows the auto-covariance of the shift for a simulation using the two-stage procedure without restoring force ($\xi = 0$) and one with the critical value of the restoring force ($\xi = \zeta^2/4$) at otherwise identical parameters. While the critically damped simulation has a larger variance of the shift (point for $h = 0$ in Fig. 5) it also features a zero crossing with anticorrelations (negative values) during a significant interval. This makes it possible to yield the same standard error while the variance is different, as seen in Fig. 4.

B. Fluctuations in different physical regimes

The Bose-Hubbard model allows us to easily change the parameters of the model to access different physical regimes. The details of the model are discussed in Appendix A. Figure 6 shows the statistics of the walker number and the shift in the equilibrium phase of an FCIQMC simulation as a function of the system size. The Hilbert space dimension grows rapidly with system size from 462 for $N = 6$ particles in $M = 6$ lattice sites to 6.9×10^{20} for 20 particles in 20 sites according to Eq. (A3). With a walker population of $\bar{N}_w \approx 10^5$, the systems up to $M = 10$ have smaller linear spaces than available walkers and thus are well sampled, whereas the Hilbert space dimension rapidly exceeds the walker number for the larger systems.

Figure 6 also shows data for ground states with different interaction strengths: a Mott insulator state with strong interactions $U/J = 6$, and a superfluid state with much weaker interactions $U/J = 1$. We see that the variance of the walker num-

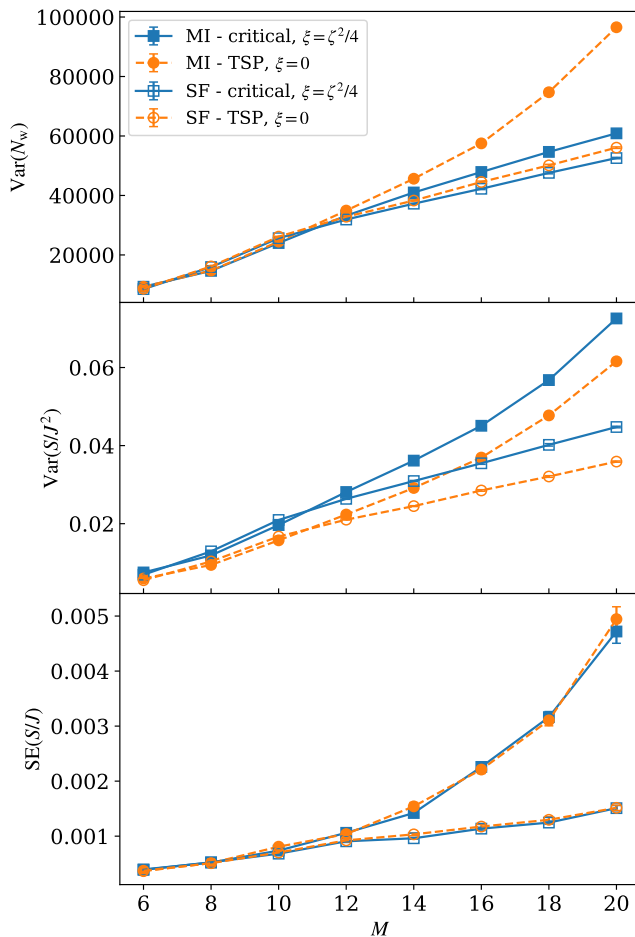


FIG. 6. Statistics of the Monte Carlo sampling in the equilibrated regime comparing the population control by the single-stage procedure with the restoring force set to critical damping ($\xi = \zeta^2/4$) and the two-stage procedure (TSP) without restoring force ($\xi = 0$). Two distinct physical regimes for the Bose–Hubbard model with unit filling factor are considered: the Mott insulating (MI, $U/J = 6$, filled markers) and superfluid (SF, $U/J = 1$, empty markers). The parameters used are $\delta\tau = 0.001J^{-1}$, and $\zeta = 0.08$ for both procedures. For all data here the walker population is equilibrated to $\overline{N}_w = 10^5 \pm 200$. One million time steps are used to obtain statistically meaningful results. Error bars are mostly within the markers.

ber and the shift as well as the standard error of the shift have very similar values for both physical states and both walker population control procedures with or without forcing with the fluctuations of the shift being slightly larger in the procedure with forcing than they are without forcing for all system sizes. The data clearly separate between the Mott insulator and superfluid state for the larger system sizes.

The data for the standard error shows that consistently the two population control procedures give the same quality of Monte Carlo data for the shift estimator, which further confirms the observation made in the previous section. The rapid increase in the standard error of the shift for the Mott insulator with system size indicates that this state becomes more diffi-

cult to sample with the FCIQMC sampling procedure, and this is also reflected by increasing fluctuations of the shift and the walker number. As discussed in more detail in Appendix A, the Mott insulator state has a single dominant configuration and many small coefficients for other configurations whereas the superfluid state is more evenly spread across Hilbert space, see also Fig. 7. A remarkable difference between the unforced and forced population control procedures is seen in the variance of the walker number in the top panel of Fig. 6. A rapid growth with system size for the Mott insulator with the unforced (original FCIQMC) procedure is reduced to a much more moderate increase with the forced procedure. Excessive fluctuations of the shift come with a cost of memory resources that have to be provided for the largest expected demand, and thus it is very desirable to suppress these fluctuations, as the forced shift-update procedure does.

VII. CONCLUSION

The newly proposed shift-update procedure (4) with the forcing strength set to the value of critical damping was shown to effectively control the walker number by adjusting it to a pre-defined parameter value N_t . The fluctuations of the walker number are reduced compared to the original procedure without forcing term, while the quality of the Monte Carlo simulation and the shift energy estimator are unaffected by the procedure or the strength of the damping coefficient. Varying the damping coefficient ζ was shown to have opposite effects on the variances of the shift and particle number. The new procedure is simpler than the original one as it removes the necessity for two simulation stages. Moreover it is easy to implement in any FCIQMC code.

An additional feature of the walker population dynamics in fermionic systems is an annihilation plateau in the walker number that emerges during Stage 1 in some cases while the shift is kept constant [6, 26]. The observation and detection of the annihilation plateau is sometimes used as an indicator that the sign problem has been mitigated and that stochastic estimators are reliable. It is possible that a single-stage shift-update procedure with forcing term could mask an annihilation plateau and make it less easily detectable. In this case, one could still perform a first simulation stage with constant shift until the plateau is detected before turning on the shift-update procedure of Eq. (4) in order to stabilise the walker number at a desired value. In many modern applications of FCIQMC where the initiator approach is used [21, 22], no annihilation plateaus appear anyway and the situation is more similar to the bosonic FCIQMC simulations presented in this work, where walker annihilation is absent.

DATA AVAILABILITY

The data that support the findings of this study are available from the corresponding author upon reasonable request. The `Rimu.jl` program can be obtained at <https://github.com/joachimbrand/Rimu.jl>.

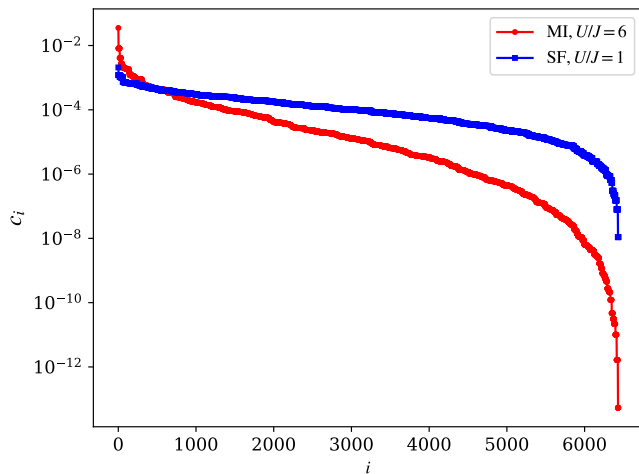


FIG. 7. The coefficients of the \mathbf{c}_0 vector for the Mott insulating (MI, red dots, $U/J = 6$) and superfluid ground state (SF, blue squares, $U/J = 1$), ordered by magnitude. The coefficient vector was normalised with the one-norm $\|\mathbf{c}_0\|_1 = 1$. The system size is $M = N = 8$ and the dimension of Hilbert space is 6435.

ACKNOWLEDGMENTS

We are grateful to Ali Alavi for enlightening discussions and encouragement. JB and EP acknowledge the hospitality of the Max-Planck Institute for Solid State Research during the early development of the FCIQMC code for bosons. This work was supported by the Marsden Fund of New Zealand (Contract No. MAU1604), from government funding managed by the Royal Society of New Zealand Te Apārangi. We also acknowledge support by the New Zealand eScience Infrastructure (NeSI) high-performance computing facilities in the form of a merit project allocation and a software consultancy project.

Appendix A: The Bose-Hubbard model

The Bose-Hubbard Hamiltonian for a one-dimensional chain of M lattice sites is written as

$$H = -J \sum_{i=1}^M \left(\hat{a}_i^\dagger \hat{a}_{i+1} + \hat{a}_{i+1}^\dagger \hat{a}_i \right) + \frac{U}{2} \sum_{i=1}^M \hat{n}_i (\hat{n}_i - 1), \quad (\text{A1})$$

where \hat{a}_i^\dagger (\hat{a}_i) is the creation (annihilation) operator for a particle at site i with bosonic permutation relations $[\hat{a}_i, \hat{a}_j^\dagger] = \delta_{ij}$ and $[\hat{a}_i, \hat{a}_j] = 0$, and $\hat{n}_i = \hat{a}_i^\dagger \hat{a}_i$ is the number operator. Periodic boundary conditions imply that $\hat{a}_{M+1} \equiv \hat{a}_1$. The total particle number $\hat{N} = \sum_{i=1}^M \hat{n}_i$ is a good quantum number and in our simulation we set it to a fixed value $\hat{N} = N$. The first term in Eq. (A1) represents particle hopping to nearest neighbour sites with hopping strength J , and the second term is an on-site interaction with strength parameter U . The Bose-Hubbard model is a non-trivial many-body problem. It has been realised experimentally with ultra-cold atoms in optical lattices [31], with quantum gas microscopes allowing single-atom-level configuration readout [32].

In order to represent the model Hamiltonian as a matrix, we use an occupation number basis (also Fock states, or configurations) in real space

$$|n_1, n_2, \dots, n_M\rangle = \prod_{i=1}^M \frac{1}{\sqrt{n_i!}} \left(\hat{a}_i^\dagger \right)^{n_i} |\text{vac}\rangle, \quad (\text{A2})$$

with fixed particle number $N = \sum_{i=1}^M n_i$. The number of independent basis states with N particles in M lattice sites and thus the dimension of the matrix \mathbf{H} is

$$\dim = \binom{M+N-1}{M}. \quad (\text{A3})$$

It can be easily adjusted, as N and M are just parameters of the model and the code.

In the thermodynamic limit ($M, N \rightarrow \infty$), the one-dimensional Bose-Hubbard model features a quantum phase transition between a Mott-insulating phase characterised by an integer number of particles per lattice site and a gapped excitation spectrum to a gapless superfluid phase [28]. While states with non-integer filling factor N/M are always superfluid, the phase transition happens for unit filling $N = M$ at a value of $U/J \approx 3.5$, where larger values correspond to the Mott insulator and smaller values to the superfluid phase.

As all off-diagonal matrix element of the Bose-Hubbard Hamiltonian are non-positive, and thus the matrix is stoquastic [39], the annihilation of walkers in FCIQMC algorithm will not be triggered. This allows us to bypass the “annihilation plateau” and avoid the QMC sign-problem, hence to focus on the dynamics that is solely controlled by the equation of the shift. In Figure 7 we show the coefficients of the ground state eigenvector \mathbf{c}_0 for two specific states of a finite system that are deep inside the Mott-insulating and superfluid regimes, respectively. The Mott-insulating state has a single dominant configuration $\prod_{i=1}^M \hat{a}_i^\dagger |\text{vac}\rangle$ in addition to many small-magnitude coefficients while the superfluid state is much more evenly spread out across Hilbert space.

[1] J Carlson, Stefano Gandolfi, and Alexandros Gezerlis, “Quantum Monte Carlo approaches to nuclear and atomic physics,” *Prog. Theor. Exp. Phys.* **2012**, 1A209 (2012), arXiv:1210.6659.

[2] David M. Ceperley and Lubos Mitás, “Quantum Monte Carlo Methods in Chemistry,” in *New Methods Comput. Quantum...*, Vol. XCIII (1996) pp. 1–38.

- [3] W. M C Foulkes, L. Mitas, R J Needs, and G Rajagopal, "Quantum Monte Carlo simulations of solids," *Rev. Mod. Phys.* **73**, 33–83 (2001).
- [4] R. J. Needs, M. D. Towler, N. D. Drummond, and P. López Ríos, "Continuum variational and diffusion quantum Monte Carlo calculations," *J. Phys. Condens. Matter* **22**, 023201 (2010), arXiv:1002.2127.
- [5] Trygve Helgaker, Poul Jørgensen, and Jeppe Olsen, *Molecular Electronic-Structure Theory* (John Wiley & Sons, Ltd, Chichester, UK, 2000).
- [6] George H. Booth, Alex J.W. Thom, and Ali Alavi, "Fermion monte carlo without fixed nodes: A game of life, death, and annihilation in Slater determinant space," *Journal of Chemical Physics* **131**, 054106 (2009).
- [7] James J. Shepherd, George Booth, Andreas Grüneis, and Ali Alavi, "Full configuration interaction perspective on the homogeneous electron gas," *Phys. Rev. B - Condens. Matter Mater. Phys.* **85**, 081103 (2012), arXiv:1109.2635.
- [8] C. J. Umrigar, "Observations on variational and projector Monte Carlo methods," *J. Chem. Phys.* **143**, 164105 (2015).
- [9] N. S. Blunt, Simon D. Smart, George H. Booth, and Ali Alavi, "An excited-state approach within full configuration interaction quantum Monte Carlo," *J. Chem. Phys.* **143**, 134117 (2015).
- [10] N. S. Blunt, Ali Alavi, and George H. Booth, "Krylov-Projected Quantum Monte Carlo Method," *Phys. Rev. Lett.* **115**, 050603 (2015), arXiv:1409.2420.
- [11] N. S. Blunt, T. W. Rogers, J. S. Spencer, and W. M. C. Foulkes, "Density-matrix quantum Monte Carlo method," *Phys. Rev. B* **89**, 245124 (2014).
- [12] Péter Jeszenszki, Ulrich Ebling, Hongjun Luo, Ali Alavi, and Joachim Brand, "Eliminating the wave function singularity for ultracold atoms by similarity transformation," *arXiv Prepr.* (2020), arXiv:2002.05987.
- [13] Aron J. Cohen, Hongjun Luo, Kai Guther, Werner Dobrautz, David P. Tew, and Ali Alavi, "Similarity transformation of the electronic Schrödinger equation via Jastrow factorization," *J. Chem. Phys.* **151**, 061101 (2019).
- [14] Werner Dobrautz, Hongjun Luo, and Ali Alavi, "Compact numerical solutions to the two-dimensional repulsive Hubbard model obtained via nonunitary similarity transformations," *Phys. Rev. B* **99**, 075119 (2019), arXiv:1811.03607.
- [15] Jarrod R. McClean and Alán Aspuru-Guzik, "Clock quantum Monte Carlo technique: An imaginary-time method for real-time quantum dynamics," *Phys. Rev. A* **91**, 012311 (2015), arXiv:1410.1877.
- [16] Kai Guther, Werner Dobrautz, Olle Gunnarsson, and Ali Alavi, "Time Propagation and Spectroscopy of Fermionic Systems Using a Stochastic Technique," *Phys. Rev. Lett.* **121**, 056401 (2018), arXiv:1709.00218.
- [17] Alexandra Nagy and Vincenzo Savona, "Driven-dissipative quantum Monte Carlo method for open quantum systems," *Phys. Rev. A* **97**, 052129 (2018), arXiv:1802.05931.
- [18] George H. Booth, Simon D. Smart, and Ali Alavi, "Linear-scaling and parallelisable algorithms for stochastic quantum chemistry," *Mol. Phys.* **112**, 1855–1869 (2014), arXiv:1305.6981.
- [19] F. R. Petruzielo, A. A. Holmes, Hitesh J. Changlani, M. P. Nightingale, and C. J. Umrigar, "Semistochastic projector Monte Carlo method," *Phys. Rev. Lett.* **109**, 230201 (2012).
- [20] N. S. Blunt, Simon D. Smart, J. A. F. Kersten, J. S. Spencer, George H. Booth, and Ali Alavi, "Semi-stochastic full configuration interaction quantum Monte Carlo: Developments and application," *J. Chem. Phys.* **142**, 184107 (2015).
- [21] Deidre Cleland, George H Booth, and Ali Alavi, "Communications: Survival of the fittest: accelerating convergence in full configuration-interaction quantum Monte Carlo." *J. Chem. Phys.* **132**, 041103 (2010).
- [22] Khaldoon Ghanem, Alexander Y. Lozovoi, and Ali Alavi, "Unbiasing the initiator approximation in full configuration interaction quantum Monte Carlo," *J. Chem. Phys.* **151**, 224108 (2019).
- [23] Nick S. Blunt, "Communication: An efficient and accurate perturbative correction to initiator full configuration interaction quantum Monte Carlo," *J. Chem. Phys.* **148**, 221101 (2018), arXiv:arXiv:1804.09528v2.
- [24] Adam A. Holmes, Hitesh J. Changlani, and C. J. Umrigar, "Efficient Heat-Bath Sampling in Fock Space," *J. Chem. Theory Comput.* **12**, 1561–1571 (2016), arXiv:1512.03757.
- [25] Verena A. Neufeld and Alex J. W. Thom, "Exciting Determinants in Quantum Monte Carlo: Loading the Dice with Fast, Low-Memory Weights," *J. Chem. Theory Comput.* **15**, 127–140 (2019).
- [26] J S Spencer, N S Blunt, and W M C Foulkes, "The sign problem and population dynamics in the full configuration interaction quantum Monte Carlo method." *J. Chem. Phys.* **136**, 054110 (2012), arXiv:1110.5479v3.
- [27] C. J. Umrigar, M. P. Nightingale, and K. J. Runge, "A diffusion Monte Carlo algorithm with very small time-step errors," *The Journal of Chemical Physics* **99**, 2865–2890 (1993).
- [28] Matthew P. A. Fisher, Peter B. Weichman, G. Grinstein, and Daniel S. Fisher, "Boson localization and the superfluid-insulator transition," *Phys. Rev. B* **40**, 546–570 (1989).
- [29] Christian Gross and Immanuel Bloch, "Quantum simulations with ultracold atoms in optical lattices," *Science* **357**, 995–1001 (2017).
- [30] D. Jaksch, C. Bruder, J. I. Cirac, C. W. Gardiner, and P. Zoller, "Cold Bosonic Atoms in Optical Lattices," *Phys. Rev. Lett.* **81**, 3108–3111 (1998).
- [31] Markus Greiner, Olaf Mandel, Tilman Esslinger, Theodor W. Hänsch, and Immanuel Bloch, "Quantum phase transition from a superfluid to a Mott insulator in a gas of ultracold atoms," *Nature* **415**, 39–44 (2002).
- [32] W. S. Bakr, A. Peng, M. E. Tai, R. Ma, J. Simon, J. I. Gillen, S. Folling, L. Pollet, and M. Greiner, "Probing the Superfluid-to-Mott Insulator Transition at the Single-Atom Level," *Science* **329**, 547–550 (2010).
- [33] Rimu. j1 is available at <https://github.com/joachimbrand/Rimu.jl>.
- [34] Kai Guther, Robert J. Anderson, Nick S. Blunt, Nikolay A. Bogdanov, Deidre Cleland, Nike Dattani, Werner Dobrautz, Khaldoon Ghanem, Peter Jeszenszki, Niklas Liebermann, Giovanni Li Manni, Alexander Y. Lozovoi, Hongjun Luo, Dongxia Ma, Florian Merz, Catherine Overy, Markus Rampp, Pradipta Kumar Samanta, Lauretta R. Schwarz, James J. Shepherd, Simon D. Smart, Eugenio Vitale, Oskar Weser, George H. Booth, and Ali Alavi, "NECI: N -Electron Configuration Interaction with an emphasis on state-of-the-art stochastic methods," *J. Chem. Phys.* **153**, 034107 (2020), arXiv:2006.14956.
- [35] James S. Spencer, Nick S. Blunt, Seonghoon Choi, Jiří Etrych, Maria-Andreea Filip, W. M. C. Foulkes, Ruth S. T. Franklin, Will J. Handley, Fionn D. Malone, Verena A. Neufeld, Roberto Di Remigio, Thomas W. Rogers, Charles J. C. Scott, James J. Shepherd, William A. Vigor, Joseph Weston, RuQing Xu, and Alex J. W. Thom, "The HANDE-QMC Project: Open-Source Stochastic Quantum Chemistry from the Ground State Up," *J. Chem. Theory Comput.* **15**, 1728–1742 (2019).
- [36] Verena A. Neufeld and Alex J. W. Thom, "Accelerating Convergence in Fock Space Quantum Monte Carlo Methods," *J. Chem.*

- Theory Comput.* **16**, 1503–1510 (2020), [arXiv:1910.05210](#).
- [37] H Flyvbjerg and H G Petersen, “Error estimates on averages of correlated data,” *J. Chem. Phys.* **91**, 461–466 (1989).
- [38] Marius Jonsson, “Standard error estimation by an automated blocking method,” *Phys. Rev. E* **98**, 043304 (2018).
- [39] Sergey Bravyi and Barbara Terhal, “Complexity of Stoquastic Frustration-Free Hamiltonians,” *SIAM J. Comput.* **39**, 1462–1485 (2010), [arXiv:0806.1746](#).